Interconnection and Damping Assignment Passivity for the Control of PV/Battery Hybrid Power Source in Islanded Microgrid

Nidhal Khefifi, Azeddine Houari, Mohamed Machmoum, Malek Ghanes

Interconnection and Damping Assignment Passivity for the Control of PV/Battery Hybrid Power Source in Islanded Microgrid

Nidhal Khefifi *‡, Azeddine Houari *, Mohamed. Machmoum *, Malek Ghanes**

* IREENA Laboratory, University of Nantes, Saint-Nazaire, France

** LS2N Laboratory, Ecole Centrale de Nantes, Nantes, France

(nidhal.khefifi@etu.univ-nantes.fr, Azeddine.Houari@univ-nantes.fr, Mohamed.Machmoum@univ-nantes.fr, Malek.Ghanes@ls2n.fr)

‡ Corresponding Author; First Author, IREENA – CRTT 37 boulevard de l'université
BP 406, 44602 Saint-Nazaire Cedex, Tel: +33 2 40 17 26 02, Fax: +33 2 40 17 26 18, nidhal.khefifi@etu.univ-nantes.fr

Abstract- This work proposes an Interconnection and Damping Assignment Passivity Based Control (IDA-PBC) to enhance power quality of an islanded Micro-grid (MG) including a photovoltaic main source (PV) and a Li-ion battery based Energy Storage System (ESS). In this MG, the PV generator-unit is controlled to provide its maximum power and the ESS-unit is controlled to ensure the desired voltage waveform at the Point of Common Coupling (PCC) and to support the PV source in order to satisfy the local loads. The IDA-PBC approach is chosen for its proprieties which allow the synthesis of asymptotically stable controllers for passive systems by the mean of the power system energy. In fact, the damping and interconnection coupling matrices of the IDA-PBC controller allows additional degree of freedoms in comparison to classical passivity controllers that enhance the convergence rapidity and the robustness under uncertainties. The mathematical model of the PV source and the Li-ion battery based ESS are presented. The power interface circuits are firstly represented through Park-coordinates then expressed in a Port-Controlled Hamiltonian (PCH) form. The obtained models are used to the design of the proposed IDA-PBC controller where the stability conditions are checked. The proposed control validity and performance are verified through comparison simulation tests with a conventional Proportional-Integral (PI) based control strategy. The obtained results show that the proposed control algorithm allows reducing the current and voltage overshoots under transient's conditions in comparison to the PI controller. Furthermore, the proposed control achieves better voltage waveform at the PCC in steady state.

Keywords Standalone AC Micro-grid, Renewable energy source, Energy storage system, Passivity based control.

Nomenclature

IDA-PBC	Interconnection and Damping Assignment Passivity Based Control
MG	Micro-Grid
PV	Photovoltaic
ESS	Energy Storage System
PCC	Point of Common Coupling
PCH	Port-Controlled Hamiltonian
PI	Proportional Integral controller
AC	Alternative current
CO2	Carbon dioxide
WT	Wind turbine
RES	Renewable energy system
E_0, V_{batt}	The battery constant and output voltage
K	The polarization constant
Q	The battery capacity
i^*	The filtred battery current.
it	The actual battery charge.
A_b	The exponential zone time constant inverse
R_b	The battery internal resistance.
I_{batt}	The current at the output of the battery
Pol_{res}	The polarization resistance
SOC	State of Charge
P&O	Perturb and observe
NiCd	Nickel-cadmium battery
NiMH	Nickel-metal hydique battery
T, E	Temperature, Illuminance
V_{cell}, I_{cell}	Voltage and current output of the solar cell
R_s, R_{sh}	Series and shunt resistance of the PV cell
V_t	The thermal voltage
V_{pv}, I_{pv}	The panel voltage and current output

P_{pv}	The power of the PV panel
I_{cell},V_{cell}	Current and voltage of a PV cell
MPPT	Maximum power point tracker
N_s, N_p	The number of series and parallel PV cell
PWM	Pulse width modulation
i_{ai}, i_{bi}, i_{ci}	The inverter real current output of DGi
v_{ai} ,v_{bi},v_{ci}	The inverter real voltage outputs of DGi
i_{di}, i_{qi}	dq-components of the real current (i_{ai}, i_{bi} and i_{ci})
v_{di} v_{qi}	The inverter voltage outputs in the dq-framework
R_{fi}, L_{fi}	The resistance and inductance of the filter i
C_f	The capacitor filter of DG1
R_L and L_L	The resistance and the inductance of the impedance connecting the filter output 1 to the PCC
v_{C_ai} ,v_{C_bi} v_{C_ci}	The real voltage at the filter output of DGi
v_{Cdi}, v_{Cqi}	The dq-components of the voltage at the filter output of DGi
i_{Ldi}, i_{Lqi}	The dq-components of the current at the filter output of DGi
ω	The angular frequency
x	The vector of state variables
u	The control action
H	The Hamiltonian function
d	The external perturbations
$\mathcal{J}$ and $\mathcal{R}$	The interconnection and damping matrices
g	The output matrice
$\mathcal{J}_d$ and $\mathcal{R}_d$	The desired interconnection and damping matrices
H_d	The desired energy function
x^*	The desired equilibrium point
$\mathcal{J}_a(x)$ and $\mathcal{R}_a(x)$	The assigned interconnection and damping matrices
H_a	The assigned energy function
i_{di}^* and i_{qi}^*	The current references for DGi
v_{Cdi}^* and v_{Cqi}^*	The voltage reference for DGi
a_{ij}, b_{ij}	The used parameters for the IDA-PBC controller
P_{PV} and Q_{PV}	The active and reactive PV power
H_{C1}, H_{V1} and H_{C}	The closed loop transfer functions of the inner and outer loop of the system.
k_{pv}, k_{iV},k_{pC1}, k_{iC1},k_{pC2},k_{iC2}	The used parameters for the inner and outer loop PI controller.
S1, S2	The used switches {0,1}
$i_{abc\text{-}ss}$; $V_{Pcc\text{-}ss}$	The inverter currents and the PCC voltage in the steady-state

1. Introduction

The widespread of renewable energy systems was motivated by environmental, economic and social strategies[1] which allow decreasing the CO2 emission, reducing the cost of energy production and improving the power quality and reliability [2]. These systems are deployed commonly as distributed generators (DG) and use diverse sources of energy [3], particularly those based on renewable energy. Among them, wind turbines (WT) and photovoltaic (PV) are the most important and used ones[4]. A cluster of these systems is defined as a MG that can operate either in grid-connected and standalone modes [5]. Indeed, thanks to the technological development progress in power converters and their control, the use of renewable energy systems (RESs) has become a key point in the development of MG [6]. However, the weather intermittence of renewable energy still presents the major handicap that may cause problems concerning stability and reliability [7]. To overcome these problems, the employ of energy storage systems (ESSs) represents an effective solution that let a flexible use and better controllability for the whole MG system[8]. Therefore, a coordinated control technique is commonly recommended to ensure the storage energy balance between ESS and the RESs to improve the micro grid's stability and reliability[9], [10].

To ensure the power quality requirements, the development of enhanced load voltage control techniques for DG systems is considered in many research works. Among others, the predictive control methods [11], the nonlinear control techniques [12] and the classical multi-loop control techniques [13], [14]. The cascaded structure using two nested PI controllers is cheap and easy to implement but needs to be linearized around the operating point. Under critical load conditions, this linearization can induce system saturation and hence reduce its stability margin [15]. To overcome the restrictions of linear controllers and ensure enhanced power quality in very large operating conditions, nonlinear control techniques are commonly used in the literature. Among these controllers we find the Feedback Linearization Control (FLC) [16], [17], backstepping [18] and Sliding Mode Control (SMC) [19], [20]. Despite the high reference tracking capacity provided using these controllers, some brittleness's are noted. For example, the FLC uses derived feedback variables that make weak the control performances at the transient instants. Moreover, this control can bother the system stability due to the zero dynamic that it can introduce to the system. SMC laws are usually built across an equivalent control based on the model and a nonlinear component presenting the correction terms. Although, the nonlinear correction term that ensure the robustness introduce chattering problems that can damage the system reliability. Recently, following the development of powerful processors and calculators, control techniques using learning methods like the interactive learning control [21] and the neural network control [22] have been implemented. However, these techniques are mostly used in systems with a slow dynamic response due to the time consumed by its complex learning algorithm. Other researchers have preferred predictive control techniques [23], These control methods are simple to implement, permit fast dynamic response and ensure flexible operations in front of various constraints and objectives [24], [25]. However, due to the employ of non-constant switching frequency in predictive control technique, an undesirable resonance can appear.

To enhance the system robustness in transient states, the feature of this paper is to propose a robust nonlinear controller based on the Interconnection and Damping Assignment Passivity Based Control (IDA-PBC) method for systems described by Port-Hamiltonian models. In this context, the Hamiltonian function represents usually the energy of the physical system and can be viewed as a Lyapunov

function[26], [27]. The employ of this approach is motivated by its proprieties allowing the synthesis of control laws guaranteeing the stability of the system by ensuring the convergence of its energy to the desired equilibrium point. For instance, it was used in [28] to control the output voltage of a boost DC-DC converter and in [29] for the control of a solid-state transformer. The design methodology of this control involves two principal steps: first, proposing a desired Hamiltonian function which ensures the control dynamic proprieties, and then synthesizing the control law by solving the matching equation.

This paper is organized as follows. In Section 2, the system modeling of each distributed generator unit and then the used model in PCH form is presented. In the third Section the synthesis of the proposed control scheme is derived. Section 4 introduces a classical PI controller in order to provide a comparative analysis. To prove the efficacy of the proposed controller, detailed simulation results are presented and debated in Section 5. Finally, a general conclusion is given in Section 6.

2. System modeling

This section presents a brief description of the studied system "Fig.1". It is composed of two distributed generators that share the supply of a common load at the PCC. In this system the PV generator injects its maximum power to the MG while the ESS controls the voltage and the frequency at the PCC bus.

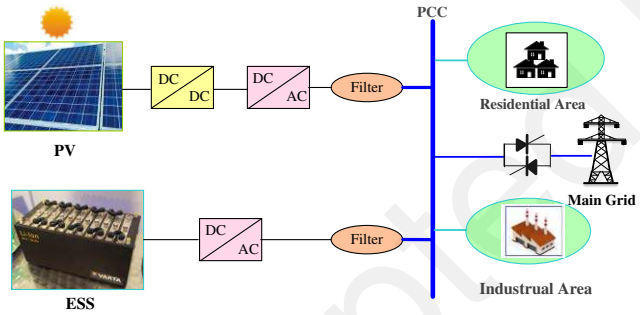

Fig. 1. Architecture of the islanded micro grid.

The following paragraphs introduces the PV and battery source models.

2.1. Battery model

The used storage system is a Li-ion Battery, this choice is driven because this technology shows a good efficiency and density compared to other usual battery like (NiCd and NiMH) [30], [31].These advantages make in progress its demand for advanced applications like in smart networks.

The model of the used battery is expressed in the following "Eq. (1)". It is composed of a constant voltage with an additional term representing the expression of battery discharge to better represent the effect of State of charge (SOC) on the battery efficiency. On the other side, instead of the real current of the battery and in order to achieve the stability, a filtered current is recommended to highlight the polarization resistance. These parameters can be derived easily from the battery datasheets or using standard dynamic test.

$$V_{batt} = E_0 - K\frac{Q}{Q-it}.it - R_b.I_{batt} + A_b\,exp(-B.it) - K\frac{Q}{Q-it}i^* \quad (1)$$

where,

- E_0 (in volt): is the battery constant voltage.
- K(in volt per ampere-hour): is the polarization constant.
- Q(in A.h): is the battery capacity.
- i^*(in A): is the filtred battery current.
- it (in A.h): is the actual battery charge.
- A_b(in A.h-1): is the exponential zone time constant inverse.
- $R_b(\Omega)$: is the battery internal resistance.
- I_{batt} (A): is the current at the output of the battery

The term $K.\left(\left(\frac{Q}{Q-it}\right).it\right)$, in the previous expression, designs the polarization voltage while the $\left(K\frac{Q}{Q-it}\right)$: is the polarization resistance Pol_{res}.

During the step of charging, the battery voltage increase brusquely from the fully charge. This comportment is indicated by modifying the polarization resistance presented in "Eq.(2)".

$$Pol_{res} = K\left(\frac{Q}{it-0.1Q}\right). \quad (2)$$

The following "Fig. 2" presents the implemented model in Matlab/Simulink of the used energy storage system.

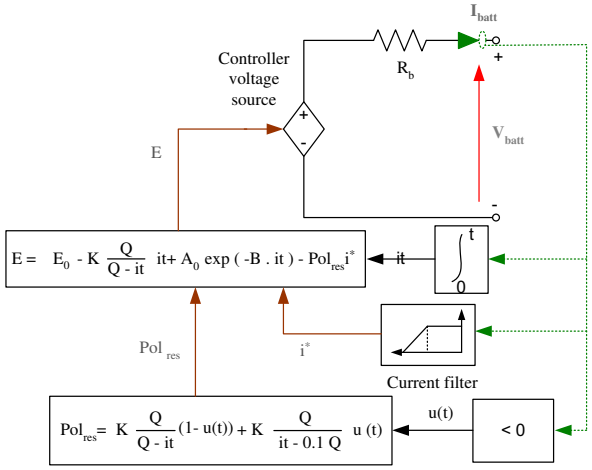

Fig. 2. Li-ion battery model.

2.2. PV panel model

The used PV panels are formed of several connected electrical solar cells. These cells are connected in particular way to reach the desired current and voltage as well as the desired rated power of the panel. In this work, the PV panel is considered as an input source that supply the AC load. The exceeded power is used to charge the used battery.

For simplest PV cell modeling purposes, the basic model usually employed in the literature is adopted. In which, the temperature effect and the dynamic due to semiconductor's junctions are neglected. The model is basically composed of P-N diode junction and it is presented in "Fig.3" [32].

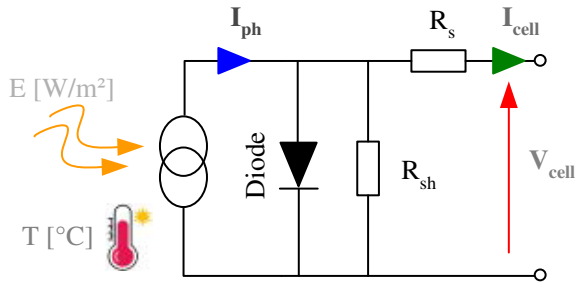

Fig. 3. Equivalent electrical scheme of a photovoltaic cell.

The proposed model can be mathematically described using the following electrical equation

$$I_{cell} = I_{ph} - I_D\left[\exp\left(\frac{V_{cell} + I_{cell}.R_s}{V_t}\right) - 1\right] - \left(\frac{V_{cell} + I_{cell}.R_s}{R_{sh}}\right) \quad (3)$$

where I_{ph} represents the photocurrent source generated proportionally by the surface isolation and the temperature. V_{cell} and I_{cell} denote respectively the output voltage and output current of the solar cell. R_s and R_{sh}represent respectively the series and shunt resistance of the model and V_t represent the thermal voltage (depending on temperature).

By solving the previous equation using "W Lambert" technique the simplified model formalism can be expressed using the current and voltage output as follow.

$$I_{cell} = \frac{V_t}{R_s}\left[R_s\frac{(I_{ph}+I_0)}{V_t} - W\left(\frac{I_0}{V_t}R_s\, exp\left(\frac{V_{cell}}{V_t}\right) exp\left(R_s\frac{(I_{ph}+I_0)}{V_t}\right)\right)\right] - \frac{V_{cell}}{R_{sh}}$$
$$V_{cell} = V_t\left[\frac{R_{sh}}{V_t}(I_{ph} + I_0 - I_{cell}) - W\left(\frac{R_{sh}.I_0}{V_t}\, exp\left(R_{sh}\frac{(I_{ph}+I_0-I_{cell})}{V_t}\right)\right)\right] - R_s I_{cell} \quad (4)$$

Thus, the photovoltaic voltage and current at the terminal of the PV panel are expressed respectively as $V_{pv} = N_s.V_{cell}$ and $I_{pv} = N_p.I_{cell}$, where N_s and N_p are respectively the number of series and parallel photovoltaic cell.

The following "Fig. 4" represents the characteristic $P_{pv} = f(V_{pv})$ for the used PV generator characterized with a rated power of 4,3kW. These characteristics are obtained in standard conditions (illumination E=1000W/m² and a temperature T=25°C).

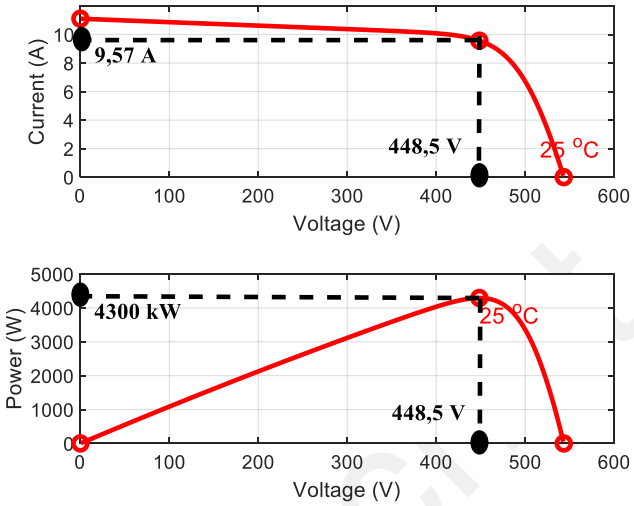

Fig. 4. Characteristic of the used PV generator in nominal conditions (T=25°C and E=1000W/m²)

This photovoltaic generator is connected to the load via a stage of boost converter allowing the adaptation of the impedance by the use of a maximum power point tracker algorithm (MPPT).

After describing and modeling the two used generator systems, the next subsection presents the modeling of the used power systems allowing the application of the proposed control.

2.3. Port-Hamiltonian modeling of the system

The circuit-scheme of the studied system is presented in "Fig. 5", in which, two DGs share the supplying of a common load. The first DG, on the left of the scheme, is used to control the voltage applied to the load. It is composed of a storage system connected to a three-phase inverter then to the load through an LC filter and a line impedance modeled by an inductance L_L in series with a resistor R_L. In this model, $L_{f1}$and R_{f1} represent respectively the first DG per-phase inductance and its internal resistance where C_f denote the filter capacitor. The second DG is composed of a photovoltaic generator connected to the PCC via a three-phase inverter then an inductance L_{f2} in series with a resistor R_{f2}. The line impedances that model the connection linking the used DG2 to the PCC are neglected since the used generators are supposed locally installed.

The objective of the proposed control is to regulate the voltage at the output of each inverter and ensure the power management between the energy produced by the PV panels and the energy available in the storage system.

The applied control for each DG unit is a low-level control. It allows to regulate the voltage at the PCC and ensure the power management between the PV panels and the ESS.

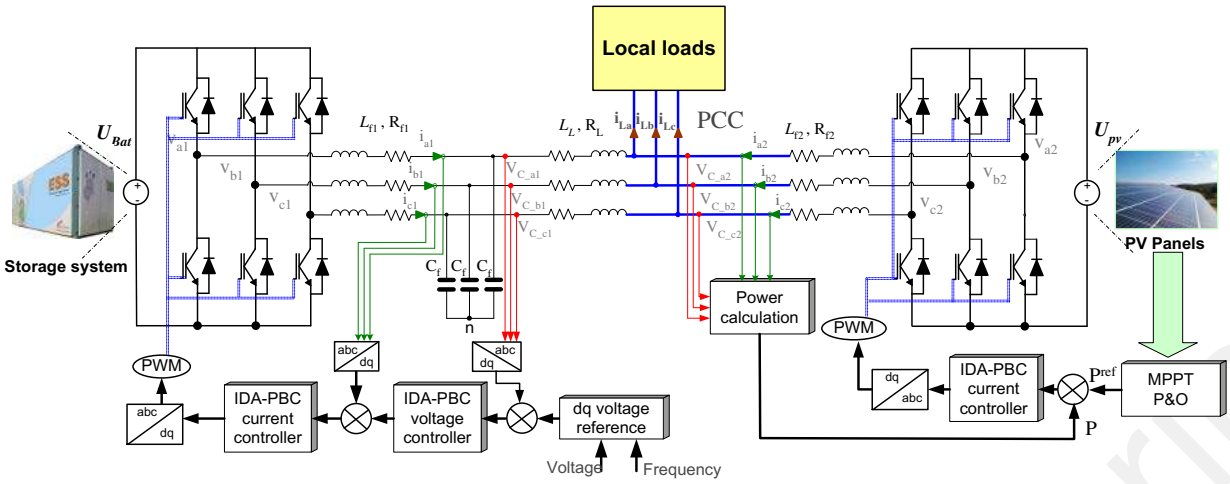

Fig. 5. Control block diagram using the passivity based control for PV panels and ESS systems.

a. Modeling of the ESS unit (DG1)

For the DG1 using the storage system, the dynamic model in the Park frame is presented in "Eq.(5)". The used system modeling in the synchronous rotating "*dq*" reference frame is employed to perform the analysis and the control of the studied system.

$$\begin{aligned} L_{f1}di_{d1}/dt &= -R_{f1}i_{d1} + L_{f1}\omega\, i_{q1} + v_{d1} - v_{Cd1} \\ L_{f1}di_{q1}/dt &= -R_{f1}i_{q1} - L_{f1}\omega\, i_{d1} + v_{q1} - v_{Cq1} \\ C_{f1}dv_{Cd1}/dt &= i_{d1} - i_{Ld1} + C_{f1}\omega\, v_{Cq1} \\ C_{f1}dv_{Cq1}/dt &= i_{q1} - i_{Lq1} - C_{f1}\omega\, v_{Cd1} \end{aligned} \quad (5)$$

In these equations, i_{d1} and i_{q1} represent the *dq*-components of the real current (i_{a1}, i_{b1} and i_{c1}), v_{d1} and v_{q1} are the inverter output voltages in the *dq*-framework, ω denote the angular frequency, v_{Cd1}, v_{Cq1} and i_{Ld1}, i_{Lq1} are respectively the *dq*-components of the filter output voltages and the filter output currents of the DG1.

Before synthesizing the controller based in IDA-PBC, the system modeling presented in "Eq.(5)", should be converted to the Port Controlled Hamiltonian model. This form, expressed in "Eq.(6)", allows thanks to its geometric structure, the synthesis of a stable and efficient control [33].

$$\begin{aligned} \dot{x} &= [\,\mathcal{J}(x) - \mathcal{R}(x)]\frac{\partial H(x)}{\partial x} + g(x)u + d \\ y &= g^T(x)\frac{\partial H(x)}{\partial x} \end{aligned} \quad (6)$$

This model arises from the Euler-Lagrange equations and represents its point of departure. where $x \in \mathcal{R}^n$ is the vector of state variables, $u \in \mathcal{R}^m$is the control action ; $m < n$, $H: \mathcal{R}^n \rightarrow \mathcal{R}$ represents the total energy stored in the system and d is a vector equivalent to the external perturbations. The control input u(x) must satisfy the following inequality.

$$\frac{\partial H(x)}{\partial x} \leq u^T y;\ H(x) \geq 0 \quad (7)$$

where H satisfies $H(0) = 0$ for all x_0 representing the initial state space conditions.

These conditions assure that the received energy is always greater or equal to the inner energy initially stored on it.

$\mathcal{R}(x) = \mathcal{R}^T(x) \geq 0$ and $\mathcal{J}(x) = -\mathcal{J}^T(x)$ are respectively the natural interconnection and damping matrices and $y \in \mathcal{R}^m$ is the outputs vector.

Converting "Eq.(5)" to the PCH form given in "Eq.(6)" is ensured by taking

$$\begin{aligned} x_1 &= [x_1 \quad x_2 \quad x_3 \quad x_4]^T \\ &= [L_{f1}i_{d1} \quad L_{f1}i_{q1} \quad C_{f1}v_{Cd1} \quad C_{f1}v_{Cq1}]^T \end{aligned} \quad (8)$$

$$\frac{\partial H_1(x)}{\partial x} = [i_{d1} \ \ i_{q1} \ \ v_{Cd1} \ \ v_{Cq1}]^T \quad (9)$$

$$u_1 = [v_{d1} \ \ v_{q1}]^T \quad (10)$$

$$d_1 = [0 \quad 0 \quad -i_{Ld1} \quad -i_{Lq1}]^T \quad (11)$$

In otherwise, the vector presented in "Eq.(8)" can be expressed differently as showing in the following "Eq.(12) "

$$x = Q\,[i_{d1} \quad i_{q1} \quad v_{Cd1} \quad v_{Cq1}]^T \quad (12)$$

where matrix $Q = diag\{L_{f1} \quad L_{f1} \quad C_{f1} \quad C_{f1}\}$. The vector x can be related to the energy function by "Eq.(13)"

$$H(x) = \frac{1}{2}x^T Q^{-1}x \quad (13)$$

The candidate energy function $H_1(x)$ of the studied system is presented in "Eq.(14)",where it is composed of the sum of the stored energy on each LC filter component.

$$\begin{aligned} H_1(x) = &\frac{1}{2}L_{f1}i_{d1}^2 + \frac{1}{2}L_{f1}i_{q1}^2 + \frac{1}{2}C_{f1}v_{Cd1}^2 \\ &+ \frac{1}{2}C_{f1}v_{Cq1}^2 \end{aligned} \quad (14)$$

This allows to have $\mathcal{J}_1(x)$ according to the form presented in "Eq.(6)":

$$\mathcal{J}_1(x) = \begin{bmatrix} 0 & L_{f1}\omega & -1 & 0 \\ -L_{f1}\omega & 0 & 0 & -1 \\ 1 & 0 & 0 & C_f\omega \\ 0 & 1 & -C_f\omega & 0 \end{bmatrix} \quad (15)$$

$$\mathcal{R}_1(\mathrm{x}) = \begin{bmatrix} R_{f1} & 0 & 0 & 0 \\ 0 & R_{f1} & 0 & 0 \\ 0 & 0 & 0 & 0 \\ 0 & 0 & 0 & 0 \end{bmatrix} \quad (16)$$

$$\mathrm{g}_1(\mathrm{x}) = \begin{bmatrix} 1 & 0 \\ 0 & 1 \\ 0 & 0 \\ 0 & 0 \end{bmatrix} \quad (17)$$

b. *Modeling of the PV unit (DG2)*

The model of the second DG is composed only by an inductance relaying the inverter to its PCC. In this case, the applied control is composed of one control loop in which the current control loop allows the management of the power.

The PV system modeling in the "*dq*" framework is presented in the following "Eq.(18)".

$$\begin{aligned} L_{f2}\frac{di_{d2}}{dt} &= -R_{f2}i_{d2} + L_{f2}\omega\, i_{q2} + v_{d2} - v_{Cd2} \\ L_{f2}\frac{di_{d2}}{dt} &= -R_{f2}i_{q2} - L_{f2}\omega\, i_{d2} + v_{q2} - v_{Cq2} \end{aligned} \quad (18)$$

To assure the current control of this model by using the IDA-PBC control, the model of "Eq.(18)" must be differently expressed to had the form presented in equation "Eq. (6)". where

$$x_2 = [x_{12} \quad x_{22}]^T = [L_{f2}i_{d2} \quad L_{f2}i_{q2}]^T \quad (19)$$

$$\frac{\partial H_2(x)}{\partial x} = [i_{d2} \quad i_{q2}\,]^T \quad (20)$$

$$u_2 = [v_{d2} \quad v_{q2}\,]^T \quad (21)$$

$$d_2 = [-v_{Cd2} \quad -v_{Cq2}]^T \quad (22)$$

Composed by the addition of the stored energy in the inductance, the candidate energy function $H_2(x)$ of the second DG is expressed in "Eq.(23)".

$$H_2(x) = \frac{1}{2}L_{f2}i_{d2}^2 + \frac{1}{2}L_{f2}i_{q2}^2 \quad (23)$$

where,

$$\mathcal{J}_2(x) = \begin{bmatrix} 0 & L_{f2}\omega \\ -L_{f2}\omega & 0 \end{bmatrix} \quad (24)$$

$$\mathcal{R}_2(x) = \begin{bmatrix} R_{f2} & 0 \\ 0 & R_{f2} \end{bmatrix} \quad (25)$$

$$g_2(x) = \begin{bmatrix} 1 & 0 \\ 0 & 1 \end{bmatrix} \quad (26)$$

3. Proposed controller design

a. Conventional IDA-PBC Approach

Ones the system is modeled in the PCH form, the controller can be synthesized. This section presents the design steps of the proposed (IDA-PBC). This process can be described in two steps. Firstly, the designer proposes a desired system function presented under its Hamiltonian form. Secondly, he calculates the control law that will be implemented.

The objective of the proposed control is to design a state-feedback control $u = \beta(x)$ such that the dynamics of the closed-loop system can guarantee the PCH form while stabilizing the system around the desired equilibrium point x^*. This objective is ensured by assigning in the closed-loop, a desired energy function $H_d(x)$ by modifying the interconnection and damping matrices.

$$\dot{x} = [\,\mathcal{J}_d(x) - \mathcal{R}_d(x)]\frac{\partial H_d(x)}{\partial x} \quad (27)$$

The index "d" defines the desired quantity, where $\mathcal{J}_d(x) = -\mathcal{J}_d^T(x)$ and $\mathcal{R}_\mathrm{d}(\mathrm{x}) = \mathcal{R}_\mathrm{d}^\mathrm{T}(x) \geq 0$ are respectively the desired interconnection and damping matrices. The desired energy function must have a strict minimum at the desired equilibrium point. For more detail, the procedure description is presented in [26]. It shows that for the assumed matrices defining the model: $\mathcal{J}(x)$, $\mathcal{R}(x)$, $\mathrm{H}(x)$ and $\mathrm{g}(x)$ and for the desired equilibrium point x^*, it is likely to define a functions $\mathcal{J}_a(x)$ and $\mathcal{R}_a(x)$ representing respectively the effect of the applied controls in the form of the interconnection and damping matrices with a vector function $K(x)$ that satisfy the matching equation "Eq.(28)" and the proprieties presented in Table 1 [29]. In this level of approach, the letter 'a' stand for the assigned term.

$$\begin{aligned} \{[\mathcal{J}(\mathrm{x}) + \mathcal{J}_a(x)] - [\mathcal{R}(\mathrm{x}) + \mathcal{R}_\mathrm{a}(\mathrm{x})]\}K(x) \\ = -[\,\mathcal{J}_\mathrm{a}(\mathrm{x}) - \mathcal{R}_\mathrm{a}(\mathrm{x})]\frac{\partial H_d(x)}{\partial x} \\ + g(x)\beta(x) + d \end{aligned} \quad (28)$$

Solving the previous matching equation allows to get the applied control to the system, where the state feedback control $u = \beta(x)$, can be attained through the matrices $\mathcal{J}_a(x)$, $\mathcal{R}_a(x)$, and the vector function $K(x)$.

Table 1. Stability properties

Structure preservation	$\mathcal{R}_d(x) = \mathcal{R}(x) + \mathcal{R}_a(x) = \mathcal{R}_d^T(x) \geq 0$ $\mathcal{J}_d(x) = \mathcal{J}(x) + \mathcal{J}_a(x) = -\mathcal{J}_d^T(x).$	(29)
Integrability:	$\frac{\partial K(x)}{\partial x} = \left[\frac{\partial K(x)}{\partial x}\right]^T$	(30)
Equilibrium assignment	$\frac{\partial H_d(x^*)}{\partial \mathrm{x}} = 0$	(31)
Lyapunov stability	$\frac{\partial^2 H_d(x^*)}{\partial \mathrm{x}^2} > 0$	(32)
Invariance of the equilibrium point	$-\left[\frac{\partial H_d(x^*)}{\partial \mathrm{x}}\right]^T \mathcal{R}_d(x^*)\left[\frac{\partial H_d(x^*)}{\partial \mathrm{x}}\right] \leq 0$	(33)

The assigned energy in the system must be defined as specified in "Eq. (34)" and "Eq. (35)".

$$H_a(x) = H_d(x) - H(x) \tag{34}$$

$$\frac{\partial H_a}{\partial x} = K(x) \tag{35}$$

The result is also a PCH system that follows the desired dynamic presented in "Eq.(27)". In this system, the designer is free to choose the matrices $\mathcal{R}_a(x)$ and $\mathcal{J}_a(x)$ to get his final controller. Therefore, the choice of $\mathcal{J}_a(x)$ is made by applying an opposite force to uncouple currents and voltages, while the $\mathcal{R}_a(x)$ is chosen to ensure a fast convergence of the system to the desired equilibrium point to enhance its dynamic.

b. Application of IDA-PBC deign to the studied system

In this section, the design outlined previously, is applied to the studied system composed of a an ESS and a PV generator. The control scheme of the proposed control is presented in the "Fig. 6".

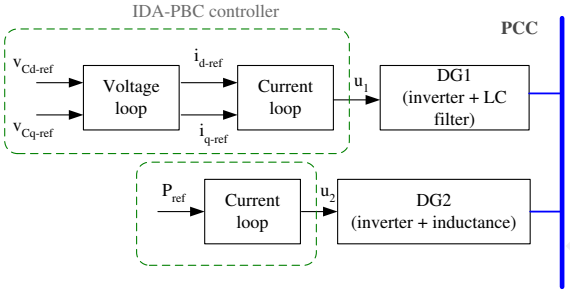

Fig. 6. Block diagram of the proposed control approach.

The first DG is composed of an inverter connected to the PCC via an LC filter, where its desired Hamiltonian function at the equilibrium point x^* is noted $H_{d1}(x)$ and had for equation the following expression.

$$\begin{aligned} H_{d1}(x) &= \tfrac{1}{2}L_{f1}(i_{d1} - i_{d1}^*)^2 + \tfrac{1}{2}L_{f1}\left(i_{q1} - i_{q1}^*\right)^2 + \\ &\tfrac{1}{2}C_{f1}(v_{Cd1} - {v_{Cd1}}^*)^2 + \tfrac{1}{2}C_{f1}\left(v_{Cq1} - {v_{Cq1}}^*\right)^2 \\ = \tfrac{1}{2L_f}(x_{11} - {x_{11}}^*)^2 &+ \tfrac{1}{2L_{f1}}(x_{21} - {x_{21}}^*)^2 + \tfrac{1}{2C_{f1}}(x_{31} \\ {x_{31}}^*)^2 &+ \tfrac{1}{2C_{f1}}(x_{41} - {x_{41}}^*)^2 \end{aligned} \tag{36}$$

For the second DG, the desired Hamiltonian function H_{d2} is represented in " Eq.(37) ".

$$\begin{aligned} H_{d2}(x) &= \tfrac{1}{2}L_{f2}(i_{d2} - i_{d2}^*)^2 + \tfrac{1}{2}L_{f2}\left(i_{q2} - i_{q2}^*\right)^2 \\ &= \tfrac{1}{2L_f}(x_{11} - {x_{11}}^*)^2 + \tfrac{1}{2L_{f1}}(x_{21} - {x_{21}}^*)^2 \end{aligned} \tag{37}$$

Following "Eq.(36)" and "Eq.(37)", the two desired Hamiltonian function satisfy the condition of equilibrium assignment "Eq.(31)" and the Lyapunov stability "Eq.(32)", where the functions K can be defined as follow.

$$\begin{aligned} \frac{\partial H_{a1}}{\partial x} = K1 = &-\frac{1}{L_{f1}}x_{11} - \frac{1}{L_{f1}}x_{21} - \frac{1}{C_{f1}}x_{31} \\ &- \frac{1}{C_{f2}}x_{41} \end{aligned} \tag{38}$$

and

$$\frac{\partial H_{a2}}{\partial x} = K2 = -\frac{1}{L_{f2}}x_{12} - \frac{1}{L_{f1}}x_{22} \tag{39}$$

It can be seen that K1 and K2 satisfies "Eq.(30)" of integrability.

Formally, to preserve the original PCH form of the interconnection and damping matrices, the candidate desired matrices for DG1 can be expressed as:

$$[\mathcal{J}_{d1}(x) - \mathcal{R}_{d1}(x)] = \begin{bmatrix} -a_{11} & 0 & a_{13} & 0 \\ 0 & -a_{22} & 0 & a_{24} \\ a_{31} & 0 & -a_{33} & 0 \\ 0 & a_{42} & 0 & -a_{44} \end{bmatrix} \tag{40}$$

where : $a_{13} = -a_{31}$, $a_{24} = -a_{42}$ and $a_{ii} \geq 0$ with $i = \{1, 2, 3, 4\}$.

Concerning the DG2, it can be expressed like shown in the following "Eq.(41)"

$$[\mathcal{J}_{d2}(x) - \mathcal{R}_{d2}(x)] = \begin{bmatrix} -b_{11} & 0 \\ 0 & -b_{22} \end{bmatrix} \tag{41}$$

The last step of the control synthesize is to calculate the control laws. These controls are obtained by solving the matching equations "Eq. (28)".

To conclude, two control in nested loops are to be defined for the DG1 that use the storage system: An outer loop that generates the line current references in the *dq*- framework and described in "Eq.(42)".

$$\begin{aligned} i_{d1}^* &= i_{Ldi} - C_{f1}\omega v_{Cq1}^* - a_{33}(v_{Cd1} - v_{Cd1}^*) \\ i_{q1}^* &= i_{Lq1} + C_{f1}\omega v_{Cd1}^* - a_{44}\left(v_{Cq1} - v_{Cq1}^*\right) \end{aligned} \tag{42}$$

And an inner loop presented by "Eq. (43)" that creates the input voltage references of the inverter.

$$\begin{aligned} v_{Cd1}^* &= -a_{11}(i_{d1} - i_{d1}^*) + v_{d1} - R_{f1}i_{d1} + L_{f1}\omega i_{q1} \\ v_{Cq1}^* &= -a_{22}\left(i_{q1} - i_{q1}^*\right) + v_{q1} - R_{f1}i_{q1} - L_{f1}\omega\, i_{d1} \end{aligned} \tag{43}$$

For the second DG only one control loop is applied which ensure the currents regulation. The same procedure is applied and the control laws are.

$$\begin{aligned} v_{Cd2}^* &= -b_{11}(i_{d2} - i_{d2}^*) + v_{d2} - R_{f2}i_{d2} + L_{f2}\omega i_{q2} \\ v_{Cq2}^* &= -b_{22}\left(i_{q2} - i_{q2}^*\right) + v_{q2} - R_{f2}i_{q2} - L_{f2}\omega\, i_{d2} \end{aligned} \tag{44}$$

The "*dq*" current references applied to this loop are obtained from the power transfer flow. It allows getting the better management of the power between the two connected DGs to better share the available power.

The power flow in the second DG justify the following system expression.

$$\begin{aligned} P_{PV} &= v_{Cd1}i_{d2} + v_{Cq2}i_{q2} + R_{f2}(i_{d2}^2 + i_{q2}^2) \\ Q_{PV} &= v_{Cq1}i_{d2} - v_{Cd1}i_{q2} + L_{f2}\omega(i_{d2}^2 + i_{q2}^2) \end{aligned} \tag{45}$$

In witch, P_{PV} and Q_{PV} represent respectively the active and reactive power at the output of the PV source by using the MPPT algorithm. In the second DG, Neglecting the resistance R_{f2} and the impedance L_{f2} allows solving the system of equations "Eq.(45)". The obtained current references are

presented in "Eq. (46)" and "Eq. (47)". It is obtained by assuming $i_{q2} = i_{q2}^*$, $i_{d2} = i_{d2}^*$, $v_{Cq1} = v_{Cq1}^*$ and $v_{Cd1} = v_{Cd1}^*$.

$$i_{d2}^* = \frac{P_{PV}.v_{Cd1}^* + Q_{PV}.v_{Cq1}^*}{v_{Cd1}^{*2} + v_{Cq1}^{*2}} \quad (46)$$

$$i_{q2}^* = \frac{P_{PV}.v_{Cq1}^* - Q_{PV}.v_{Cd1}^*}{v_{Cd1}^{*2} + v_{Cq1}^{*2}} \quad (47)$$

4. Conventional PI Controller

To verify and prove the effectiveness of the proposed IDA-PBC controller, a PI controller with a decoupled technique to avoid the non-linearity of the systems is proposed. This control is based on two nested loops: an outer voltage loop and an inner current loop. The control laws of the inner and outer loops for DG1 are determined by the following expressions:

$$\begin{aligned} i_{d1}^* &= G_V(s)(v_{Cd1} - v_{Cd1}^*) + i_{Ld1} - C_f\omega v_{Cq1} \\ i_{q1}^* &= G_V(s)(v_{Cq1} - v_{Cq1}^*) + i_{Lq1} + C_f\omega v_{Cd1} \\ v_{d1}^* &= G_C(s)(i_{d1}^* - i_{d1}) + R_{f1}i_{d1} - L_{f1}\omega\, i_{q1} + v_{Cd1} \\ v_{q1}^* &= G_C(s)(i_{q1}^* - i_{q1}) + R_{f1}i_{q1} + L_{f1}\omega\, i_{d1} + v_{Cq1} \end{aligned} \quad (48)$$

For DG2, the implemented control is composed of one loop presented in "Eq. (49)".

$$\begin{aligned} v_{d2}^* &= G_C(s)(i_{d2}^* - i_{d2}) + R_{f2}i_{d2} - L_{f2}\omega\, i_{q2} + v_{Cd2} \\ v_{q2}^* &= G_C(s)(i_{q2}^* - i_{q2}) + R_{f2}i_{q1} + L_{f2}\omega\, i_{d2} + v_{Cq2} \end{aligned} \quad (49)$$

In this equation $G_V(s)$ and $G_C(s)$ represent the PI transfer functions of the outer and inner loops. The corresponding closed loop transfer functions of the inner ($H_{C1}(s)$) and outer loop ($H_{V1}(s)$)

$$H_{C1}(s) = \frac{(k_{pC}/L_{f1})s + (k_{iC}/L_{f1})}{s^2 + (k_{pC}/L_{f1})s + (k_{iC}/L_{f1})} \quad (50)$$

$$H_{V1}(s) = \frac{(k_{pV}/C_f)s + (k_{iV}/C_f)}{s^2 + (k_{pV}/C_f)s + (k_{iV}/C_f)} \quad (51)$$

Respectively for the current loop on DG2, $H_{C1}(s)$ have the following expression:

$$H_{C2}(s) = \frac{(k_{pC}/L_{f2})s + (k_{iC}/L_{f2})}{s^2 + (k_{pC}/L_{f2})s + (k_{iC}/L_{f2})} \quad (52)$$

To ensure better rejection of the disturbance and avoid the interaction between the two control loops, the bandwidth of the outer loop (ω_V) is fixed to be ten time less that the current loop (ω_C). The used control is implemented by means of the pole placement technique. The used parameters for the inner and outer loop are calculated respectively as follow:

$$\begin{aligned} k_{pV} &= 2\,mC_f\omega_V \\ k_{iV} &= C_f\,\omega_V^2 \end{aligned} \quad (53)$$

$$\begin{aligned} k_{pC1} &= 2\,mL_{f1}\omega_C \\ k_{iC1} &= L_{f1}\,\omega_C^2 \end{aligned} \quad (54)$$

$$\begin{aligned} k_{pC2} &= 2\,mL_{f2}\omega_C \\ k_{iC2} &= L_{f2}\,\omega_C^2 \end{aligned} \quad (55)$$

The inner loop bandwidth is set equal to 2000 rad/s, the outer loop bandwidth to 200 rad/s and the damping factor "m" is set to 0,7.

5. Simulation results

To validate the performance of the proposed control method, comparative simulation tests with a PI controller is performed using MATLAB/Simulink software. For this simulation test, two DG units composed of one PV source and an ESS that supply two local loads as shown in Fig. 7.

The rated power of each load is around 3kW and the test scenario is described as follow:

- For the supplied load:
  - ➢ From t=0 to 0.15 s, the system supplies a load of 3 kW.
  - ➢ From t=0.15 to 0.2 s, connection of the second load, the value of the local load is doubled to attend 6 kW.
- For the illumination profile:
  - ➢ From t=0 to t= 0.05s, the PV panels receive an illumination of 750W / m².
  - ➢ From t=0.05 to 0.1 s, decrease of the received illumination from 750 to 500W / m².
  - ➢ From t=0.1to 0.2 s, increase of the received illumination to reach 1000W / m².

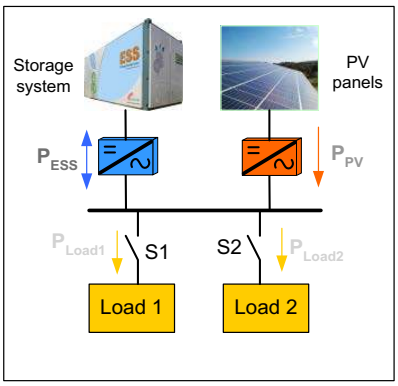

Fig. 7. The electrical system used in the simulation.

Notice that for proposed tests are performed under following hypotheses:

- The battery state of charge is kept on the tolerable operating interval between 95% and 30% where the battery is not overcharged or discharged.

- The ambient temperature is considered equal to 25 °C.

- The dynamic due to semiconductor's junctions on the PV panels are neglected.

- The presented results illustrate only the power quality enhancement of the proposed control under short-time working operation.

The main specification of the used system and controller parameters are resumed in the following Table 2 and Table 3.

Table 2. System parameters

Parameters	Value
$L_{f1} = L_{f2}$	3 mH
$R_{f1} = R_{f2}$	0,1 Ω
C_f	50 µF
U_{Batt}	400V
Switching frequency	10 kHz
P_{PV-nom}	4,3 kW

Table 3. Control parameters

PI Controller		IDA-PBC Controller	
Parameter	***Value***	***Parameter***	***Value***
k_{iV}	2.82	$a_{11} = a_{22}$	10
k_{pV}	0.024	$a_{33} = a_{44}$	1
$k_{iC1} = k_{iC2}$	16922	$a_{13} = -a_{31}$	1
$k_{pC1} = k_{pC2}$	14.15	$a_{24} = -a_{42}$	1
		$b_{11} = b_{22}$	10

The used illuminance profile in this simulation is presented in the following Fig. 8.

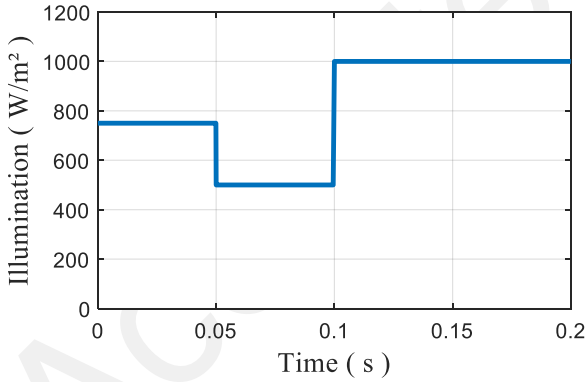

Fig. 8. Illumination profile.

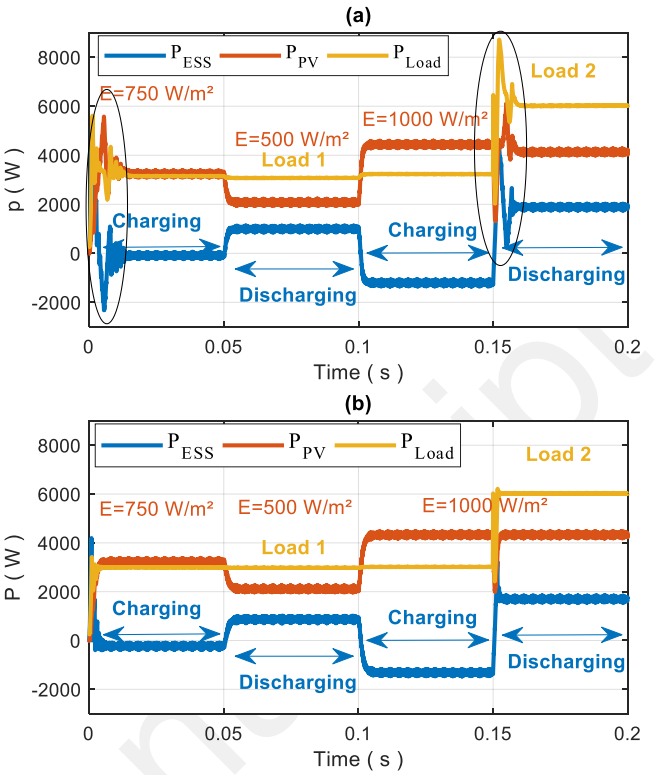

Fig. 9. Performance of the real power in the islanded AC micro grid: (a) classical PI controller ;(b) proposed IDA-PBC controller.

The PI and the proposed control performances are presented respectively in "Fig. 9"-a and "Fig. 9-b". These figures present simultaneously the power at the output of the PV generator, the power of the energy storage system and the requested load power at the PCC.

It can be seen that when the PV source produce enough power to ensure the needs of the loads, the excess power is stored in the used battery in order to charge it. Whereas, in the case where the power produced by PV panels is insufficient for the load demands, the used battery provides the missing power for the loads by discharging itself.

As can be seen, the proposed control allows better disturbance rejection and a smoother power transition at the instant of start-up and the moment of load variation.

"Fig. 10-a" and "Fig. 10-b" show respectively the currents in the ESS and the PV generator using the PI controller, compared to "Fig. 10-c" and "Fig. 10-d" that show the same measured variables when using the proposed controller.

These two figures show that the currents in the PV generator and in the storage system using the conventional controller present a larger overshoot and a wide time response than those when employing the proposed IDA-PBC control. This observation is very much seen at the instance of load application (t=0.15s) as well at the startup time. Consequently, such overshoot affects the wave of currents and voltages of the load at the PCC bus as it is presented in "Fig. 11".

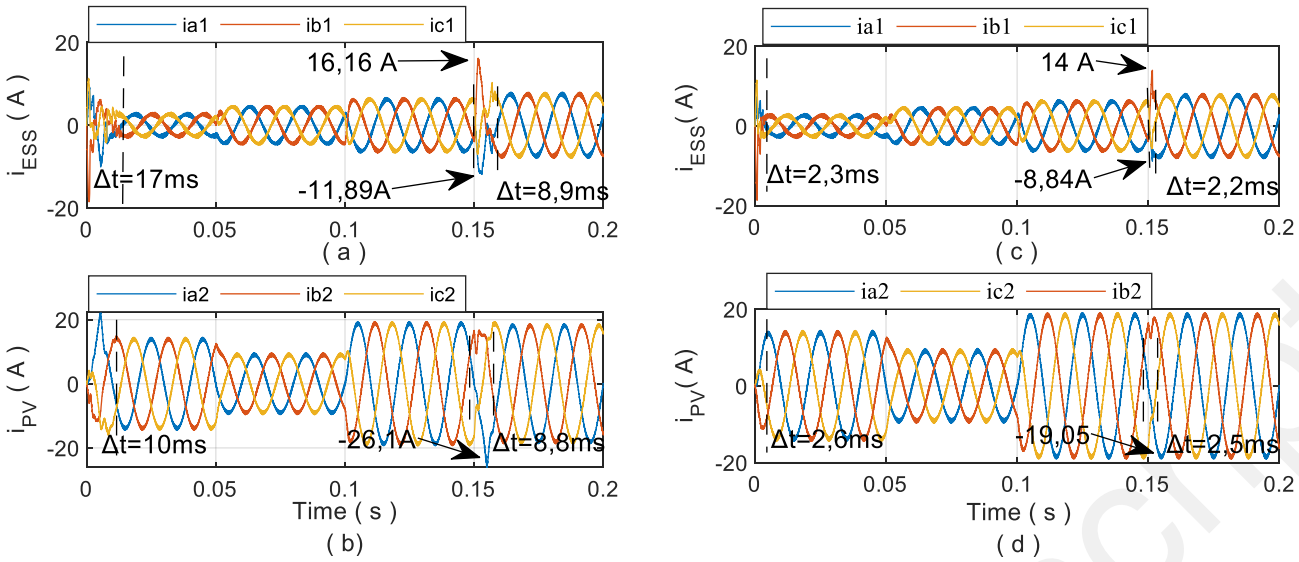

Fig. 10. Conventional PI control: (a) currents of ESS, (b) PV panels; Proposed IDA-PBC control: (c) currents of ESS, (d) PV panels.

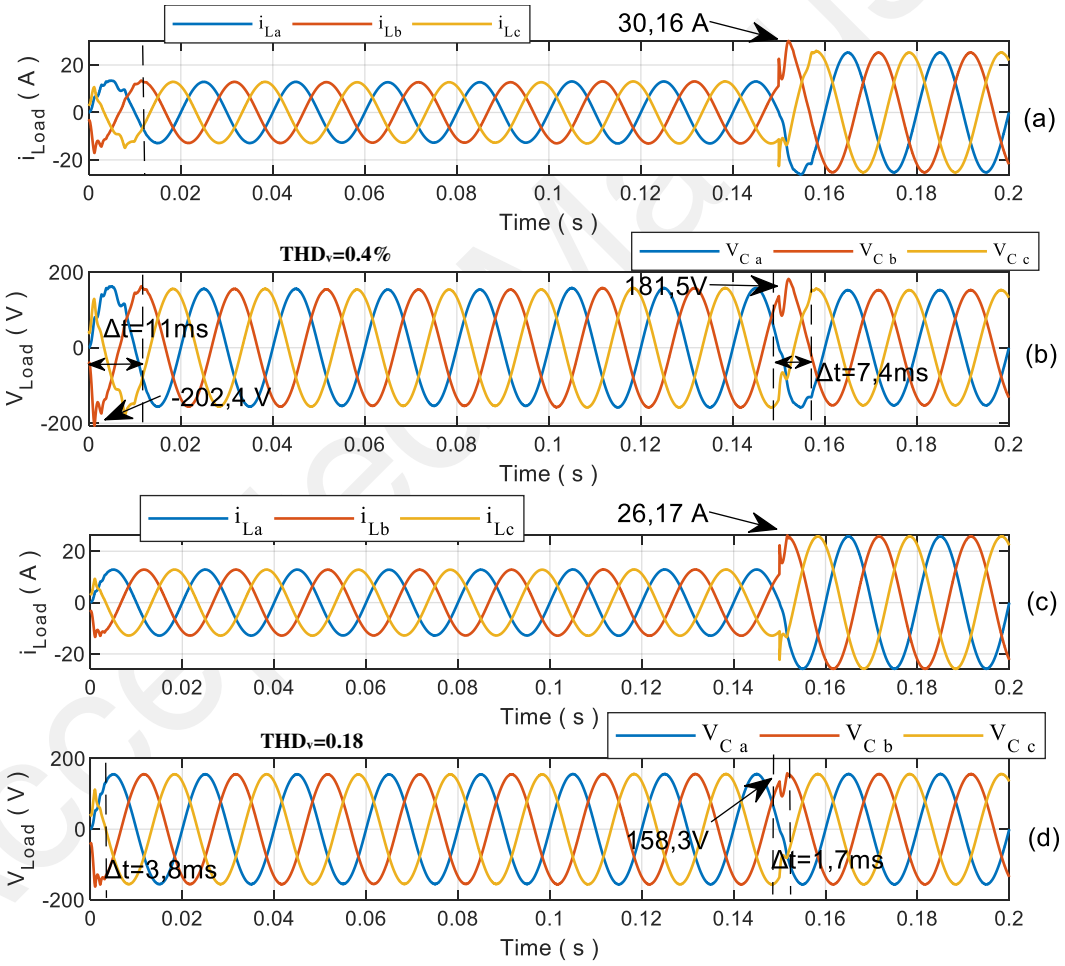

Fig. 11. Injected currents and voltages for the local load using the PI Controller: (a) currents, (b) voltages; using IDA-PBC controller: (c) currents, (d) voltages.

The injected load currents and voltages are presented respectively in "Fig. 11-a" and "Fig. 11-b" for the PI controller and in "Fig. 11-c" and "Fig. 11-d" for the proposed IDA-PBC controller. These comparisons prove that using the proposed controller, we obtain the fast response time and the less overshot. It can be seen that for the voltage wave we can

decrease the response time using the proposed controller from 7,4ms to 1,7ms in front of step load from 3kW to 6kW. At the same time, we can reduce respectively the voltage and current amplitude from 181.5V to 158.3V and from 30,16A to 26,14A at the instant of the disturbance. For the start-up time and thanks to the developed control, it is possible to reduce the response time from 11ms to 3,8ms.

In steady-state, it can be observed that the voltage THD rate obtained by the IDA-PBC controller is equal to 0.18% while that using PI controller is 0.4%, showing more the effectiveness of the proposed controller.

These results prove the effectiveness of the proposed control to get better power management between the PV generator and the Li-ion battery based Energy Storage System. It can be seen that the proposed control allows to improve the performance for the current and voltage responses by assuring low overshoot, short settling time and zero steady-state error.

Discussion

The performances of the proposed IDA-PBC compared with the used PI controller are summarized in the following Table. 4. As it can be appreciated, the IDA-PBC shows better performance compared to the classical PI controller. In steady-state, it can be observed that the voltage THD rate obtained by the IDA-PBC controller is equal to 0.18% while that using PI controller is 0.4%. These values are not excessive but it shows that the proposed controller achieves better voltage waveform. Also, it can be noticed that the disturbance rejection ability is enhanced with the proposed control scheme. It allows to have the short time response with the small overshot at transient states.

Table 4. PI and IDA-PBC controller performances

Regime		***Test Specification***		**Controller**	
				PI	**IDA-PBC**
Steady state	**Test**	**Voltage THD**	**PCC**	*0.4%*	*0.18%*
Dynamic tests	***Start*-up**	***Current response time***	***ESS***	*17ms*	*2.3ms*
			PV	*10ms*	*2.6ms*
		Current variation $\Delta i_{max} = (i_{max}-i_{abc\text{-}ss})$	***ESS***	*15,64A*	*15,59*
			PV	*7.64A*	*0.04A*
	Step load	***Voltage response time***	***PCC***	*7,4ms*	*1,7ms*
		Current variation $\Delta i_{max} = (i_{max}-i_{abc\text{-}ss})$	***ESS***	*8.5A*	*5.9A*
			PV	*7.7A*	*0.65A*
		Voltage peak $\Delta V_{max} = (V_{Pcc\text{-}max}-V_{Pcc\text{-}ss})$	***PCC***	*181.5V*	*158.3V*

6. Conclusion

This paper has presented a robust IDA-PBC control strategy to enhance the power quality of an islanded MG composed of a PV generator with a Li-ion battery based energy storage system. The PV source is controlled to provide its available maximum power to the local loads while the energy storage system is controlled to support the PV source and ensure voltage amplitude and frequency control at the PCC. The use of this passivity-based approach allows a physically interpretation of the control where the energy is shaped to converge asymptotically to the equilibrium reference. The structure of the IDA-PBC allows to ensure fast convergence while enhancing the robustness thanks to the damping and interconnection matrices. The ESS and PV sources are mathematically modeled then their power systems are formulated in the Hamiltonian form before synthesizing the used control laws. The proposed control stability is checked and its validity and performance are verified through comparative simulation tests with a conventional PI based control technique. The obtained results are analyzed. They illustrate that the proposed controller allows better disturbance rejection at transient conditions while ensuring a reduced voltage THD at the PCC under steady state operation.

References

[1] Y. Gui, B. Wei, M. Li, J. M. Guerrero, and J. C. Vasquez, "Passivity-based coordinated control for islanded AC microgrid," Applied Energy, vol. 229, pp. 551–561, Nov. 2018.

[2] P. Sreekumar and V. Khadkikar, "Adaptive Power Management Strategy for Effective Volt–Ampere Utilization of a Photovoltaic Generation Unit in Standalone Microgrids," IEEE Transactions on Industry Applications, vol. 54, no. 2, pp. 1784–1792, Mar. 2018.

[3] M. R. Miveh, M. F. Rahmat, A. A. Ghadimi, and M. W. Mustafa, "Control techniques for three-phase four-leg voltage source inverters in autonomous microgrids: A

review," Renewable and Sustainable Energy Reviews, vol. 54, pp. 1592–1610, Feb. 2016.

[4] A. Mukherjee, K. S, and P. S. Subudhi, "Investigation of a PV fed Improved Smart Home EV Battery Charging System using Multi Output Hybrid Converter," International Journal of Renewable Energy Research (IJRER), vol. 9, no. 2, pp. 692–703, Jun. 2019.

[5] A. H. Hubble and T. S. Ustun, "Composition, placement, and economics of rural microgrids for ensuring sustainable development," Sustainable Energy, Grids and Networks, vol. 13, pp. 1–18, Mar. 2018.

[6] N. Khefifi, A. Houari, M. Ait-Ahmed, M. Machmoum, and M. Ghanes, "Robust IDA-PBC Based Load Voltage Controller for Power Quality Enhancement of Standalone Microgrids," in IECON 2018 - 44th Annual Conference of the IEEE Industrial Electronics Society, 2018, pp. 249–254.

[7] N. Khefifi, A. Houari, M. Machmoum, and M. Ghanes, "Interconnection and Damping Assignment Passivity Based Control for Power Sharing in Islanded Micro-Grids," in 2018 7th International Conference on Renewable Energy Research and Applications (ICRERA), 2018, pp. 1157–1161.

[8] H. Zhao, Q. Wu, S. Hu, H. Xu, and C. N. Rasmussen, "Review of energy storage system for wind power integration support," Applied Energy, vol. 137, pp. 545–553, Jan. 2015.

[9] J. Hu, Y. Xu, K. W. Cheng, and J. M. Guerrero, "A model predictive control strategy of PV-Battery microgrid under variable power generations and load conditions," Applied Energy, vol. 221, pp. 195–203, Jul. 2018.

[10] H. Wen, H. Yu, and Y. Hu, "Modeling and analysis of coordinated control strategies in AC microgrid," in 2016 IEEE International Conference on Renewable Energy Research and Applications (ICRERA), 2016, pp. 702–707.

[11] H. T. Nguyen, E. Kim, I. Kim, H. H. Choi, and J. Jung, "Model Predictive Control with Modulated Optimal Vector for a Three-Phase Inverter with an LC Filter," IEEE Transactions on Power Electronics, vol. 33, no. 3, pp. 2690–2703, Mar. 2018.

[12] D. Pullaguram, S. Mishra, N. Senroy, and M. Mukherjee, "Design and Tuning of Robust Fractional Order Controller for Autonomous Microgrid VSC System," IEEE Transactions on Industry Applications, vol. 54, no. 1, pp. 91–101, Jan. 2018.

[13] M. Shahparasti, M. Mohamadian, A. Yazdian, A. A. Ahmad, and M. Amini, "Derivation of a Stationary-Frame Single-Loop Controller for Three-Phase Standalone Inverter Supplying Nonlinear Loads," IEEE Transactions on Power Electronics, vol. 29, no. 9, pp. 5063–5071, Sep. 2014.

[14] Jing Wang and A. Monti, "Current control of grid connected inverter with LCL filter utilizing two degree-of-freedom control," in 2013 International Conference on Renewable Energy Research and Applications (ICRERA), 2013, pp. 967–972.

[15] S. Mohagheghi, Y. del Valle, G. K. Venayagamoorthy, and R. G. Harley, "A Proportional-Integrator Type Adaptive Critic Design-Based Neurocontroller for a Static Compensator in a Multimachine Power System," IEEE Transactions on Industrial Electronics, vol. 54, no. 1, pp. 86–96, Feb. 2007.

[16] S. Pugliese, R. A. Mastromauro, and S. Stasi, "Simplified feedback linearization control of a single-phase photovoltaic NPC converter in direct-quadrature rotating reference frame," in 2015 International Conference on Renewable Energy Research and Applications (ICRERA), 2015, pp. 1369–1375.

[17] G. Lou, W. Gu, W. Sheng, X. Song, and F. Gao, "Distributed Model Predictive Secondary Voltage Control of Islanded Microgrids With Feedback Linearization," IEEE Access, vol. 6, pp. 50169–50178, 2018.

[18] R. Wai, C. Lin, W. Wu, and H. Huang, "Design of backstepping control for high-performance inverter with stand-alone and grid-connected power-supply modes," IET Power Electronics, vol. 6, no. 4, pp. 752–762, Apr. 2013.

[19] D. P. Andrea, D. N. L. Pio, and M. Santolo, "Super twisting sliding mode control of smart-inverters grid-connected for PV applications," in 2017 IEEE 6th International Conference on Renewable Energy Research and Applications (ICRERA), 2017, pp. 793–796.

[20] A. Houari, A. Djerioui, A. Saim, M. Ait-Ahmed, and M. Machmoum, "Improved control strategy for power quality enhancement in standalone systems based on four-leg voltage source inverters," IET Power Electronics, vol. 11, no. 3, pp. 515–523, 2018.

[21] W. Lu, K. Zhou, D. Wang, and M. Cheng, "A General Parallel Structure Repetitive Control Scheme for Multiphase DC–AC PWM Converters," IEEE Transactions on Power Electronics, vol. 28, no. 8, pp. 3980–3987, Aug. 2013.

[22] H.-K. Kang, C.-H. Yoo, I.-Y. Chung, D.-J. Won, and S.-I. Moon, "Intelligent Coordination Method of Multiple Distributed Resources for Harmonic Current Compensation in a Microgrid," Journal of Electrical Engineering and Technology, vol. 7, pp. 834–844, Nov. 2012.

[23] F. Yazdi and S. H. Hosseinian, "A novel 'Smart Branch' for power quality improvement in microgrids," International Journal of Electrical Power & Energy Systems, vol. 110, pp. 161–170, Sep. 2019.

[24] J. S. Lim, C. Park, J. Han, and Y. I. Lee, "Robust Tracking Control of a Three-Phase DC–AC Inverter for UPS Applications," IEEE Transactions on Industrial Electronics, vol. 61, no. 8, pp. 4142–4151, Aug. 2014.

[25] H. Heydari-doostabad and R. Ghazi, "A new approach to design an observer for load current of UPS based on Fourier series theory in model predictive control system,"

International Journal of Electrical Power & Energy Systems, vol. 104, pp. 898–909, Jan. 2019.

[26] R. Ortega and E. García-Canseco, "Interconnection and Damping Assignment Passivity-Based Control: A Survey," European Journal of Control, vol. 10, no. 5, pp. 432–450, Jan. 2004.

[27] N. Khefifi, A. Houari, M. Machmoum, M. Ghanes, and M. Ait-Ahmed, "Control of grid forming inverter based on robust IDA-PBC for power quality enhancement," Sustainable Energy, Grids and Networks, vol. 20, p. 100276, Dec. 2019.

[28] F. Serra, G. Magaldi, L. Martin Fernandez, L. Guillermo, and C. De Angelo, "IDA-PBC controller of a DC-DC boost converter for continuous and discontinuous conduction mode," IEEE Latin America Transactions, vol. 16, no. 1, pp. 52–58, Jan. 2018.

[29] R. V. Meshram, M. Bhagwat, S. Khade, S. R. Wagh, A. M. Stanković, and N. M. Singh, "Port-Controlled Phasor Hamiltonian Modeling and IDA-PBC Control of Solid-State Transformer," IEEE Transactions on Control Systems Technology, vol. 27, no. 1, pp. 161–174, Jan. 2019.

[30] P. García, J. P. Torreglosa, L. M. Fernández, and F. Jurado, "Viability study of a FC-battery-SC tramway controlled by equivalent consumption minimization strategy," International Journal of Hydrogen Energy, vol. 37, no. 11, pp. 9368–9382, Jun. 2012.

[31] S. Njoya Motapon, L.-A. Dessaint, and K. Al-Haddad, "A Comparative Study of Energy Management Schemes for a Fuel-Cell Hybrid Emergency Power System of More-Electric Aircraft," IEEE Transactions on Industrial Electronics, vol. 61, no. 3, pp. 1320–1334, Mar. 2014.

[32] J. P. Ram, H. Manghani, D. S. Pillai, T. S. Babu, M. Miyatake, and N. Rajasekar, "Analysis on solar PV emulators: A review," Renewable and Sustainable Energy Reviews, vol. 81, pp. 149–160, Jan. 2018.

[33] R. Ortega and J. G. Romero, "Robust integral control of port-Hamiltonian systems: The case of non-passive outputs with unmatched disturbances," Systems & Control Letters, vol. 61, no. 1, pp. 11–17, Jan. 2012.